Multi-spectral False Color Shadow Detection

Mustafa Teke[1], Emre Başeski[1], Ali Özgün Ok[2],
Barış Yüksel[1], and Çağlar Şenaras[1]

[1] HAVELSAN A.Ş., Eskişehir Yolu 7.km 06520, Ankara, Turkey
{mteke,ebaseski,byuksel,csenaras}@havelsan.com.tr
[2] Middle East Technical University, Department of Geodetic and Geographic Information Technologies, 06531, Ankara, Turkey
oozgun@metu.edu.tr

Abstract. With the availability of high-resolution commercial satellite images, automated analysis and object extraction became even a more important topic in remote sensing. As shadows cover a significant portion of an image, they play an important role on automated analysis. While they degrade performance of applications such as image registration, shadow is an important cue for information such as man-made structures. In this article, a shadow detection algorithm that makes use of near-infrared information in combination with RGB bands is introduced. The algorithm is applied on an application for automated building detection.

Keywords: Shadow detection, building detection, near-infrared, false color.

1 Introduction

Aerial and satellite images contain varying amount of shadows depending on the acquisition time, surface properties and number of objects on the surface that cast shadow. Shading is considered as an important visual cue as it can be used to reveal the shape of an object from a single image (see e.g., Zhang et al. (1999) for a review). Therefore, detecting shaded areas on a remotely sensed image can give valuable information for automated detection of man-made objects.

As the sun radiates light, photons collide with particles in the air and scatter. The scattering of light is inversely proportional to the wavelength of photons and this phenomenon is explained by Rayleigh scattering (Rees (1993)). In visible spectrum, blue component of light scatters most. Therefore, blue band has higher values than green and red bands in shaded areas. Additionally, shaded areas appear darker than their neighbors. Shadow detection algorithms usually exploit color values in different color spaces to make use of these facts. In Polidorio et al. (2003), shadow detection on satellite and aerial images is performed by applying different threshold values to Saturation and Intensity differences. Sarabandi et al. (2004) exploits properties of c1c2c3 and suggests that c1c2c3 color space produces better results than RGB and HSV. Both works use manual thresholds and the results vary significantly depending on these thresholds. Tsai (2006) uses different color spaces (HSV, HSI, HCV, YIQ, YCbCr)

U. Stilla et al. (Eds.): PIA 2011, LNCS 6952, pp. 109–119, 2011.

for shadow detection from aerial images where different Ratio Maps for each of these color spaces are compared. The method argues that the best performance is obtained using Hue and Intensity ratio in HSI color space and an automated thresholding is applied to the Ratio Map by using Otsu's method (Otsu (1979)). In Chung et al. (2009), an improvement to Tsai's method is proposed which uses a new ratio map and an automated successive thresholding scheme. Note that, these methods work on the RGB interval of the spectrum and do not exploit the potential of Near-Infrared (NIR) band.

In NIR band, shaded areas appear dark and this fact can be used to design algorithms that can discriminate shadow and other dark regions with a better performance. For example, Fredembach and Süsstrunk (2010) proposes an automatic shadow detection method which uses NIR band as an additional cue to create a darkness map that is based on both NIR and intensity.

Although the color of a shadow region is supposed to be dark, this darkness varies extensively (even in the same image) depending on the surface characteristics and material properties. The fundamental idea behind the work in this article is to darken the shaded areas on an image by removing the blue band as it scatters most and treating green, red, NIR bands as RGB. This new false-color space is then converted into HSI and an automated thresholding is applied on the Ratio Map histogram. The algorithm has been tested on IKONOS images with 1 meter and GeoEye images with 0.5 meter resolution. Also in Sect. 4, the potential of the proposed method is demonstrated on an application which makes use of shadow information for automated building detection.

2 Proposed Method

In this article, an automated shadow detection method that is based on visible and NIR part of the spectrum is proposed. In shadow areas, Blue band scatters most. As a result, pixel values in shadow areas have higher values in Blue band than the other bands such as Red or NIR. Also, Blue channel carries less information than Red and NIR bands as it spans a narrower portion of the spectrum. By removing the Blue band and shifting RGB color space to NIR band, one can obtain a false-color space (NIR-R-G) where the shadow areas become darker. We use the reflectance properties of shadows in this false-color space in order to detect shadows. The work-flow of the algorithm is illustrated in Fig. 1 and output of different steps of the algorithm is shown in Fig. 2.

Once the NIR-R-G image is obtained, it is converted into HSI color space (see Fig. 2-(b) for an example). Based on Polidorio et al. (2003), a difference map is calculated by using Equation 1.

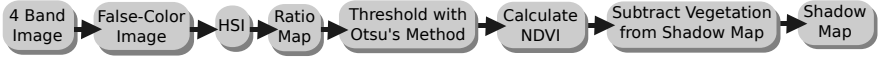

Fig. 1. Algorithm Steps

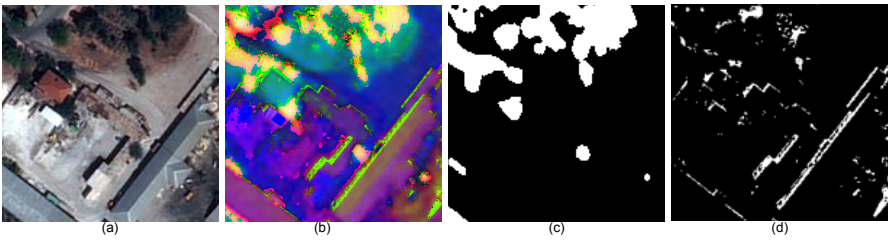

Fig. 2. Different steps of the algorithm. **(a)** Original image, **(b)** False color in HSI space, **(c)** Vegetation map, **(d)** Shadow detection result.

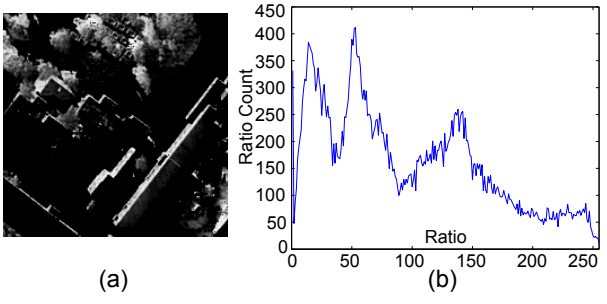

Fig. 3. (a) Ratio Map of the image that is shown in Fig. 2 **(b)** Histogram of the Ratio Map

$$S - I, \tag{1}$$

where S is normalized saturation and I is normalized intensity. Vegetation and dark objects have similar S-I values. In order to distinguish these areas, a Ratio Map is calculated by dividing the difference map into S+I (Equation 2) since vegetated areas have higher S and I values compared to shaded areas. A sample Ratio Map and its histogram is shown Fig. 3.

$$\frac{S - I}{S + I}, \tag{2}$$

After the calculation of the Ratio Map, an automated threshold is applied to its histogram by using Otsu's method. As an example, Otsu's method finds the threshold as 100 for the histogram that is shown in Fig. 3-(b).

The automated thresholding scheme detects shadows and vegetation at the same time. Therefore, the vegetated areas are supposed to be eliminated to obtain only the shadow areas. By using Red and NIR bands, vegetation can be detected based on Normalized Difference Vegetation Index (NDVI) (see e.g., Tucker (1979) for details). A sample Vegetation Map is shown in Fig. 2-(c). To obtain the final Shadow Map, the Vegetation Map is used to eliminate the vegetated areas (see Fig. 2-(d) for an illustration).

3 Experimental Results

In this section, the evaluation of the proposed algorithm is presented. The experiments have been performed on a series of images whose shaded areas were labeled manually. Three IKONOS images with 1 meter (first three columns of Fig. 4) and one GeoEye image (fourth column of Fig. 4) with 0.5 meter resolution have been used. The labeled ground-truth images for the IKONOS images are presented on the second row of Fig. 4. Note that, the GeoEye image was evaluated only visually. The numerical evaluation of IKONOS images for different shadow detection algorithms is presented in Table 1, 2 and 3. The performance of the algorithms has been evaluated based on precision (Equation 3) and recall (Equation 4) measurements.

$$\text{Precision} = \frac{\text{True Positive}}{\text{True Positive} + \text{False Positive}}, \tag{3}$$

$$\text{Recall} = \frac{\text{True Positive}}{\text{True Positive} + \text{False Negative}}, \tag{4}$$

where True Positive regions are labeled as shadow and detected as shadow, False Positive regions are labeled as non-shadow and detected as shadow, True Negative regions are labeled as non-shadow and detected as non-shadow, and False Negative regions are labeled as shadow and detected as non-shadow.

Table 1. Evaluation of different algorithms on the image that is at the first column of Fig. 4

	True Positive	*True Negative*	*False Positive*	*False Negative*	*Precision*	*Recall*
Proposed	6587	189067	27361	12092	19.40%	35.26%
Polidorio	10893	187210	29218	7786	27.15%	58.31%
Tsai	15888	144080	72348	2791	18.00%	85.05%
Chung	8716	191325	25103	9963	25.77%	46.66%
Fredembach	4996	184299	32129	13683	13.45%	26.74%

Before discussing the numerical results, we would like to stress some important points about the visual results of the algorithms. As water appears dark both in visible and NIR spectrum, all algorithms detect water as shadow. Therefore, the number of False Positives increases drastically which reduces the Precision for the first and second images for all algorithms. Also, except the proposed method, the shadows of man-made objects are either missing or there are too many False Positives that make these shadows difficult to use for automated object extraction.

The results on the third column of Fig. 4 can be used as a fair evaluation criteria for precision as there is no water on the image. As the Table 3 suggests,

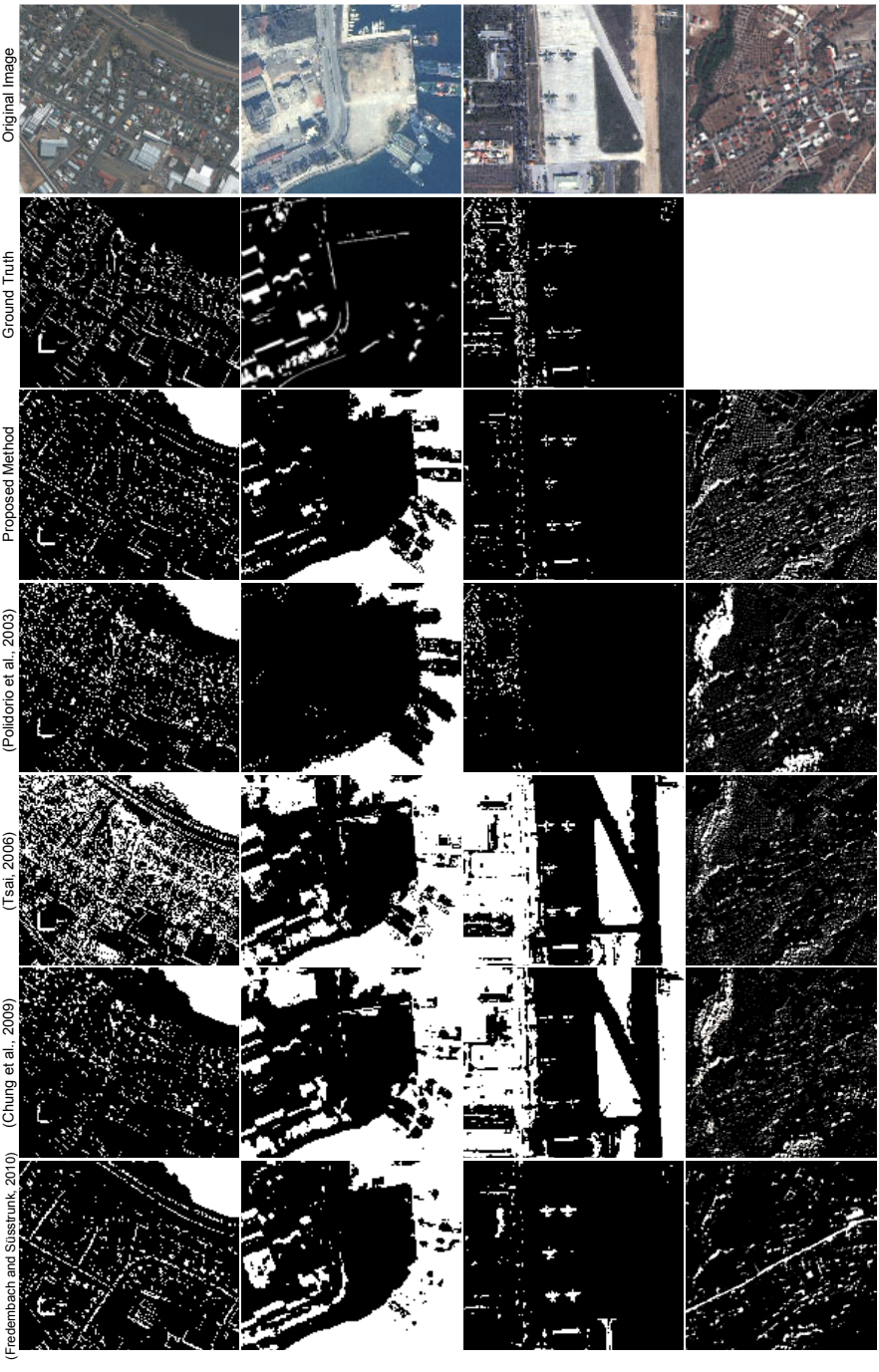

Fig. 4. Evaluation of different algorithms on IKONOS and GeoEye images

Fig. 5. Shadow detection results on various IKONOS and GeoEye images

Table 2. Evaluation of different algorithms on the image that is at the second column of Fig. 4

	True Positive	*True Negative*	*False Positive*	*False Negative*	*Precision*	*Recall*
Proposed	1726	56515	22924	4165	7.00%	29.29%
Polidorio	190	60379	19060	5701	0.98%	3.22%
Tsai	4868	46200	33239	1023	12.77%	82.63%
Chung	4664	47215	32224	1227	12.64%	79.17%
Fredembach	3904	48604	30835	198	11.23%	95.17%

Table 3. Evaluation of different algorithms on the image that is at the third column of Fig. 4

	True Positive	*True Negative*	*False Positive*	*False Negative*	*Precision*	*Recall*
Proposed	1561	220586	588	11919	72.63%	11.58%
Polidorio	3297	219904	1270	10183	72.19%	24.45%
Tsai	13214	101268	119906	266	9.92%	98.02%
Chung	12108	124210	96964	1372	11.10%	89.82%
Fredembach	3471	217204	3970	10009	46.64%	25.74%

the proposed method and Polidorio et al. (2003) give the best results for precision. On the other hand, Polidorio et al. (2003) is quite threshold dependent, and both the precision and the recall values can decrease drastically (see Table 2) depending on the threshold. While the algorithm in Tsai (2006) produces relatively high results for recall, the precision value in Table 3 and the visual results in Fig. 4 suggest that the algorithm produces too many False Positives. The algorithm in Chung et al. (2009) introduces an improvement on the algorithm in Tsai (2006) for both precision and recall but still the number of False Positives is higher than the rest of the algorithms. As mentioned in Sect. 1, the algorithm in Fredembach and Süsstrunk (2010) uses NIR band and the effect of illumination is less compared to the algorithms that use only visible spectrum.

When the visual and the numerical results are compared, one can observe that the main difference between the proposed method and the method in Fredembach and Süsstrunk (2010) is the number of False Positives. The proposed method finds more certain shadows than the method in Fredembach and Süsstrunk (2010). This leads to slightly more sparse shadows with a better precision for the proposed method.

More visual results of the proposed method is presented in Fig. 5. The first three rows are GeoEye images with 0.5 meter resolution and the last two rows are IKONOS images with 1 meter resolution. Visual inspection suggests that the proposed method can detect both artificial and natural shadows.

4 Building Detection as an Application

In this section, the potential of the proposed shadow detection algorithm is illustrated on a building detection scenario. Building detection is one of the

challenging problems of automated target detection in remote sensing applications. A wide range of algorithms and models have been developed for automatic building extraction from monocular images. An exceptional survey can be found in Mayer (1999). Later, an extended version of this survey bounded in Mayers format was conducted by Unsalan and Boyer (2005). The trends followed within the state-of-the-art of building extraction can be found in Gruen et al. (1995, 1998); Baltsavias et al. (2001).

The main difficulty of building detection comes from the fact that the shape, color and textural properties of buildings change drastically from one image to another. The only property that is common about buildings is that their elevation is higher than the terrain surface. As mentioned in Sect. 1, shadows can be used as a fundamental cue to acquire the related height information from monocular images. Therefore, so far, manipulation of various shadow maps to estimate the position and height of the buildings is a widely accepted approach (see e.g., Huertas and Nevatia (1988); Irvin and McKeown (1989); Sirmacek and Unsalan (2008); Akcay and Aksoy (2010)).

In our building detection application, we exploit the shadow map produced by the proposed method. Buildings are extracted by using their neighboring shadows. In general, this type of extraction requires the knowledge of the exact sun direction and the sun angular elevation on a per image basis. With the knowledge of *(i)* the latitude, longitude, and height information of the image part being investigated, and *(ii)* the date/time the image was acquired, it is possible to compute the angles of sun azimuth and zenith (Reda and Andreas (2007)) during the image acquisition. Thereafter, the computed azimuth information can be utilized to infer buildings from the related shadow map.

In this study, we extracted the buildings using an approach similar to the one presented in Akcay and Aksoy (2010). The spatial relationships between the shadows and the buildings can be defined relative to each other. For sure, this relationship must be modeled with respect to a direction which is defined by the computed azimuth information. Given a shadow object (B) and the opposite direction of the computed azimuth angle (α), potential building landscape $\beta_{\alpha,\lambda,\tau}(B)$ around the shadow object along the given direction can be defined as a fuzzy function in image space (Cinbis and Aksoy (2007)):

$$\beta_{\alpha,\lambda,\tau}(B)(x) = (B \oplus \upsilon_{\alpha,\lambda,\tau})(x) \cap B^c \tag{5}$$

$$\upsilon_{\alpha,\lambda,\tau}(x) = g_\lambda(\frac{2}{\pi}\Theta_\alpha(x,o)max\{0, 1 - \frac{\|\overrightarrow{ox}\|}{\tau}\}$$

where, υ is a fuzzy structuring element, g is a one-dimensional Bezier curve function with an inflection point λ, $\|\overrightarrow{ox}\|$ is the Euclidean distance of an image point x to the center (o) of the structuring element, $\Theta_\alpha(x,o)$ is the angle between the vector $\overrightarrow{ox}$ and the unit vector along the direction α, τ is a threshold corresponding to the distance where a point is no longer attracted from the shadow object, B^c represents complement of the shadow object, and $\oplus$ defines the morphological dilation. Once the potential building landscapes are generated, the

Fig. 6. Results of our building detection algorithm which uses the proposed shadow detection algorithm

buildings are detected by combining the similar segments along the defined building landscape. In Fig. 6 a sample building detection result is presented. Note that, the shadow map given in the last column of Fig. 4 has been used for this example.

5 Conclusion

We presented an automatic multi-spectral shadow detection algorithm which takes advantage of Near Infrared Band. It obtains a darkness image based on a false color spectrum where green, red, NIR bands are used as RGB. The final shadow mask is obtained by removing vegetation from a thresholded shadow map. The proposed method has been compared with the state-of-the-art shadow detection methods and the results have been evaluated both numerically and visually. Also, the potential of the algorithm has been illustrated on an application that is based on building detection.

The proposed method detects shadows with high precision but the detection results are relatively sparse compared to the other algorithms. Although this reduces the recall values, the algorithm detects shadows for most of the objects that cast shadow on the image. Therefore, it does not detect all shadows but detects shadows for most of the objects. Another advantage of the algorithm is its independence from manual thresholds. As it has been presented in Sect. 3, finding a universal threshold is not possible and finding the image specific thresholds is crucial.

As water appears dark both in visible and NIR spectrum, the proposed algorithm detects water as shadow. On the other hand, this is a common issue for all shadow detection algorithm and a shape based post processing is required to distinguish between water and shadow. A similar problem occurs in case of dark objects such as very dark roads. Contrast stretching and image adjusting for dark images which have narrow histogram are suggested to improve detection performance. However, histogram equalization is observed to produce too many false positives since distribution of pixel values is transformed in a non-linear way.

References

Akcay, H., Aksoy, S.: Building detection using directional spatial constraints. In: IGARSS, pp. 1932–1935 (2010)

Baltsavias, E.P., Gruen, A., Van Gool, L.: Automatic Extraction of Man-Made Objects from Aerial and Space Images (III). Balkema (2001)

Chung, K.L., Lin, Y.R., Huang, Y.H.: Efficient shadow detection of color aerial images based on successive thresholding scheme. IEEE Transactions on Geoscience and Remote Sensing 47(2), 671–682 (2009)

Cinbis, R.G., Aksoy, S.: Modeling spatial relationships in images. Tech. Rep. BU-CE-0702, Department of Computer Engineering, Bilkent University, Ankara, Turkey (2007)

Fredembach, C., Süsstrunk, S.: Automatic and accurate shadow detection from (potentially) a single image using near-infrared information. IEEE Transactions on Pattern Analysis and Machine Intelligence (2010)

Gruen, A., Baltsavias, E.P., Henricsson, O.: Automatic Extraction of Man-Made Objects from Aerial and Space Images (II). Birkhauser, Boston (1998)

Gruen, A., Kubler, O., Agouris, P.: Automatic Extraction of Man-Made Objects from Aerial and Space Images. Birkhauser, Boston (1995)

Huertas, A., Nevatia, R.: Detecting buildings in aerial images. Comput. Vision Graph. Image Process. 41(2), 131–152 (1988)

Irvin, R., McKeown, D.M.: Methods for exploiting the relationship between buildings and their shadows in aerial imagery. IEEE Transactions on Systems, Man and Cybernetics 19(6), 1564–1575 (1989)

Mayer, H.: Automatic object extraction from aerial imagery–a survey focusing on buildings. Computer Vision and Image Understanding 74(2), 138–149 (1999)

Otsu, N.: A threshold selection method from gray-level histograms. IEEE Transactions on Systems, Man and Cybernetics 9(1), 62–66 (1979)

Polidorio, A.M., Flores, F.C., Imai, N.N., Tommaselli, A.M.G., Franco, C.: Automatic shadow segmentation in aerial color images. In: Proc. XVI Brazilian Symp. Computer Graphics and Image Processing, pp. 270–277 (2003)

Reda, I., Andreas, A.: Solar position algorithm for solar radiation application. Tech. Rep. NREL/TP-560-34302, National Renewable Energy Laboratory, NREL (2007)

Rees, W.G.: Physical Principles of Remote Sensing (1993)

Sarabandi, P., Yamazaki, F., Matsuoka, M., Kiremidjian, A.: Shadow detection and radiometric restoration in satellite high resoluiton images. In: Proceedings of IEEE International on IGARES 2004, Anchorage, AK, vol. 6, pp. 3744–3747 (2004)

Sirmacek, B., Unsalan, C.: Building detection from aerial images using invariant color features and shadow information. In: Proceedings of the 23rd International Symposium on Computer and Information Sciences, ISCIS 2008, pp. 1–5. IEEE, Los Alamitos (2008)

Tsai, V.: A comparative study on shadow compensation of color aerial images in invariant color models. IEEE Transactions on Geoscience and Remote Sensing 44(6), 1661–1671 (2006)

Tucker, C.J.: Red and photographic infrared linear combinations for monitoring vegetation. Remote Sensing of Environment 8(2), 127–150 (1979)

Unsalan, C., Boyer, K.: A system to detect houses and residential street networks in multispectral satellite images. Computer Vision and Image Understanding 98(3), 423–461 (2005)

Zhang, R., Tsai, P., Cryer, J., Shah, M.: Shape from shading: A survey, vol. 21(8), pp. 690–706 (August 1999)